

BNL 31971

CONF-820839--4

DESIGN CONSIDERATIONS FOR AN X-RAY MICROPROBE*

BNL--31971

M.R. Howells and J.B. Hastings
NSLS Division, Brookhaven National Laboratory, Upton, New York

DE83 000976

MASTER

ABSTRACT

The optical design of a fluorescent microprobe covering the x-ray region from 2 to 16 keV is considered for the NSLS x-ray ring. The limit on detectability is from total flux (photons/ μm^2) and several design choices are considered to match the optical system to the storage ring to maximize throughput. The tradeoffs in image quality and energy resolution of these designs have been considered and within these constraints two firm proposals are presented.

PORTIONS OF THIS REPORT ARE ILLEGIBLE. It has been reproduced from the best available copy to permit the broadest possible availability. MN ONLY

INTRODUCTION

The desirable characteristics of an x-ray microprobe have been reviewed by a number of authors^{1, 2} and have lead to the preparation of a detailed proposal³ for a microprobe beamline at the NSLS. The basic idea is to observe the fluorescent x-rays emitted following the creation of core holes by the incident beam. By scanning the sample in a suitable raster pattern it is possible to produce maps of the distribution of the elements whose characteristic x-rays are detected. Since x-rays suffer very little scattering prior to the photoelectric event which creates the core hole, it follows that the spatial resolution of the microprobe is determined entirely by the geometry of the focussed x-ray beam. In fact, we shall see that for most cases of importance it is determined by the spot size alone.

We can conclude that the usefulness of the microprobe is determined by the following characteristics:

1. Spot size and convergence angle: spatial resolution
2. Range of wavelengths produced: range of edges that are accessible
3. Monochromaticity: radiation damage level, detection statistics, element selectivity
4. X-ray flux: statistics, detectability thresholds, etc.

DISCLAIMER
This report was prepared as an account of work sponsored by an agency of the United States Government. Neither the United States Government nor any agency thereof, nor any of its employees, makes any warranty, express or implied, or assumes any legal liability or responsibility for the accuracy, completeness, or usefulness of any information, apparatus, product, or process disclosed, or represents that its use would not infringe privately owned rights. Reference herein to any specific commercial product, process, or service by trade name, trademark, manufacturer, or otherwise, does not necessarily constitute or imply its endorsement, recommendation, or favoring by the United States Government or any agency thereof. The views and opinions of authors expressed herein do not necessarily state or reflect those of the United States Government or any agency thereof.

*Work supported by the U.S. Department of Energy Contract No.

Obviously the more favorable the values of these parameters the wider the class of problems that can be studied.

In this paper we address the question of how to approach the optical design of a microprobe system. We consider the fundamental physical limitations involved and also the limitations of particular types of optical components. We then consider a particular design problem: a microprobe for the NSLS x-ray ring. The design goal in the present study is to achieve a 3μ spot for a beam covering 2-16 keV with $\lambda/\Delta\lambda \sim 50$. We show in Fig 1. why the range 2-16 keV is chosen. It is the smallest range that covers all the elements up to lead using either the K or L edges.

BRIGHTNESS CONSIDERATIONS

Our studies of how to concentrate an x-ray beam into a small spot naturally start with the requirement that the spot cannot be brighter than the source. The brightness of the source at any wavelength is the total x-ray flux divided by the product of the horizontal and vertical emittances. It will be expressed in units such as photons/sec/mm²/μstr. The fundamental law that brightness cannot be increased even in a loss-free system is also applicable separately to the horizontal and vertical emittances. In paraxial optics this law is called the Helmholtz-Lagrange Invariance Theorem and states that the product $hn\alpha$, evaluated at conjugate planes, is invariant for any ray where h is the distance from the central ray, α is the angle to the central ray and n is the refractive index of the medium. With $n = 1$ we see that the emittance, $E = h\alpha$, of the x-ray beam is the quantity of interest at the source location. At a focus in the optical system we define an acceptance A expressed similarly to E . In the plane we are considering, the fraction of the beam accepted is then A/E . We note also that if the emittance and acceptance have the same values in both planes then the fraction of the beam accepted is A^2/E^2 . In order to represent the various physical effects which limit the formation of small x-ray spots we start by plotting the emittance of the x-ray beam as a function of photon energy (Fig. 1). We use units of milliradian microns for ease of visualization.

The other lines on Fig. 1 require some explanation but first we anticipate some of the details of the beamline scheme worked out later. We consider a 300μ source and seek to demagnify it with the goal of a spot of width $x = 3\mu$. In addition, suppose we are using a plane mirror with critical angle $\theta_c(E) = \sqrt{2\delta(E)}$. The upper limit of the angular acceptance of the mirror is something like $0.5\theta_c$ so the upper limit of the acceptance A is $0.5\theta_c x$. This is plotted as "reflectance limit" in Fig. 1. We see that above about 1 keV a conventional mirror focussing to a 3μ spot cannot accept the whole beam.

The ultimate limit to imaging quality is diffraction. We know for example that even a perfect optical system of aperture width, a , will image a point source as an Airy pattern with angular half width α_D given by

$$\alpha_D = \frac{1.22\lambda}{a}$$

According to the Rayleigh criterion this is also the separation in the image plane needed to just resolve two point sources. Thus a wavefront always appears to originate from a source of finite size and the smallest possible photon beam emittance E_D is given by

$$E_D = 1.22\lambda(\text{\AA}) \quad \text{\AA} \cdot \text{radians}$$

$$\text{or } E_D = 0.122\lambda(\text{\AA}) \quad \text{mr} \cdot \mu$$

This is shown as "diffraction limit" in Fig. 1.

We may remark in passing that if a is very small the divergence, α_D is still given by the above expression and we then speak of a diffraction limited pinhole. Such a source is spatially coherent and so the curve for E_D also defines the emittance of a coherent source.

We have already suggested that the microprobe resolution may be a function of both the size and convergence angle of the x-ray beam. We can define an angle α_R which is the beam divergence angle for which the beam just grows to the spot width in the distance needed for 90% attenuation in the sample. Apparently:

$$\alpha_R = \frac{x}{L}$$

where L is the range (90% attenuation) of the x-rays in the sample. In Fig. 1 we plot $E_R = x^2/L$ the emittance corresponding to α_R for the case $x = 3\mu$ and a biological sample, the worst practical case of a low z matrix. We see that for a beam whose emittance is at the reflectance limit the resolution would be significantly impaired if a heavy element were being mapped in a biological sample using a 10-15 keV incident beam. For lower photon energies and/or denser samples the beam divergence would not limit the resolution.

OPTICAL COMPONENTS

In order to design a microprobe system we need a systematic way to determine the amount of beam which an optical component can accept. The best approach is to fit the calculated acceptance of various optical components into the framework of Fig. 1. Certainly, one way to focus x-rays to a small spot is to use a Fresnel Zone plate. For hard x-rays this is limited by the transparency of the zone plate material. We show in Fig. 1 the limit when a gold zone plate transmits 10%. We have the very clear conclusion that it is the device of choice below 1 keV but is of little use for hard x-rays. Thus, we limit our considerations to two types of components:

1. The Kirkpatrick-Baez (KB) microscope configuration.
2. A single ellipsoid of revolution.

Each of these components suffers from fundamental limitations: The KB microscope, being made from spherical surfaces suffers from spherical aberration and if a certain spot size is demanded this sets a limit to the angular acceptance. This turns out to depend on the focal length and we calculate it below. The ellipsoid of revolution has theoretically no limit to its angular acceptance and no other serious aberrations for the geometry of interest to us. However, the practical limit is determined by the range of sizes in which it can be fabricated. We consider this in detail below

THE KIRKPATRICK BAEZ MICROSCOPE

The basic idea of the KB microscope⁴ is shown in Fig. 2. Two nominally cylindrical mirrors are used, one to focus in the vertical direction, the other for the horizontal. Both mirrors reflect at a very grazing angle and for this case the cylinders can be well approximated by spherical surfaces. The usefulness of the KB microscope is based on the fact that these spherical surfaces are easily fabricated with good figure accuracy and surface smoothness. Of course, the circle is not the correct shape for the point-to-point imaging. This can only be achieved with an ellipse. However, over a limited length of the curve the circle approximates an ellipse well enough to give a point image with aberrations which are tolerable for certain purposes. We evaluate this quantitatively below. From the point of view of a microprobe we notice three important differences compared to the reflection x-ray microscope:

1. We wish to demagnify a spot so we are using the device in reverse.
2. For typical synchrotron source geometry the field of view is small compared to what would be needed for useful microscopy.
3. We have no interest in ensuring that the image should resemble the object.

The third of these is the most significant. It turns out that the major limitation of the KB microscope for creating magnified images is the aberration (peculiar to nonaxially symmetric systems) known as obliquity of field. This is the condition where the image plane lies at an angle other than 90° to the outgoing principal ray. In fact, it can be shown⁵ that if no stops are used, the image plane lies at an angle θ to the principal ray where θ is the grazing angle! This is evidently a very unfavorable condition and various aperture and field stops have been proposed^{5, 6} to improve it. However, none of these schemes have been sufficiently successful to enable the KB microscope to enter routine use for biology. It is now used in a limited way as a diagnostic tool for laser fusion and has otherwise fallen from favor.

As long ago as 1953 it was proposed by Kirkpatrick and Pattee that the KB configuration be used as a microprobe. In view of point 3 above we have no need to take account of obliquity of field for this case. Consequently, we can evaluate the device simply on the basis of the spherical aberration calculation in the original paper of Kirkpatrick and Baez.⁴

Figure 3 shows the layout and the notation. POQ is the principal ray and Q is the focus for rays near the principal ray. The question is, what is the distance S by which another ray such as PNQ' will be displaced from Q when it arrives in the receiving plane? In other words what is the width of the blurr from a point source when the mirror has finite width? According to Kirkpatrick and Baez this is given in the small angle approximation by

$$S = \frac{3Mp\alpha}{M+1} \left\{ \frac{M^2 + 2aM - 1}{M+1 - 2aM} \right\}$$

$$\text{where } a = \frac{\alpha}{1}$$

and considering the case of small M we get

$$S = \frac{3Mp\alpha^2}{1}$$

leading to

$$S = \frac{3}{2} \frac{w^2}{R}$$

For example, for a mirror with $p = 10$ m, $q = 1$ m, $i = 1^\circ$ (which implies $R = 104$ m) and half width, $w = 50$ mm we get $S = 36.0 \mu$. From exact ray tracing the correct figure is 32.5μ so the approximation is not too bad. The second mirror can be treated similarly and independently of the first.

From a functional point of view we are interested in the focal length of the device and the semi-convergence angle 2α at the spot so using $f = 1/2 Ri$ we get

$$S = \frac{3f\alpha^2}{i}$$

and the acceptance A_{KB} is given by

$$A_{KB} = S.4\alpha = 4S \sqrt{\frac{Si}{3f}}$$

We see that for given requirements for S and i the light gathering power is dependent on the focal length. We can now plot some examples on Fig. 4 to show how well the KB system could perform. We consider the case when $i = 0.75 \theta_c$ and plot two cases

$$S = 30 \mu \quad f = 1 \text{ m}$$

$$S = 3 \mu \quad f = 0.1 \text{ m}$$

They are intended to show the possible performance for stage 1 and stage 2 if we chose to achieve our desired 100:1 magnification in two stages of 10:1. (Notice that an actual mirror has a constant acceptance. What we

are plotting here are limits.) We see clearly from the plot that the KB system would be able to accept about the maximum allowed by the reflectance limit, if used for stage 1, but would involve considerable loss of flux if used for stage 2.

However, we should note that since we carried out all the calculations with the assumption of M small, these spot size and acceptance results are good for all values of M provided they are small. Therefore, the stage 2 arrangement above would work perfectly well as a single stage 100:1 condenser provided the radius R were suitably adjusted.

Finally, an advantage of the KB system is that since the mirrors are almost flat they lend themselves to use with Bragg reflectors, such as perfect crystals or multilayer coatings.¹¹ The latter has already been done by the Lawrence Livermore Laboratory group.⁷ There are possibilities for an important class of practical devices here and we now consider them in more detail.

BRAGG REFLECTORS

The use of Bragg reflectors has the important advantage of providing both monochromatization and focusing and also of removing the requirement of using grazing angles less than the critical angle.

The spot size is still controlled by aberration considerations in the same way as before but with generally larger grazing angles determined by the Bragg condition. The energy spread of such a system will be composed of the intrinsic width of the Bragg reflection combined with a width driven by the spread of Bragg angles caused by the curvature of the reflector.

The energy spread for symmetric reflection is easily calculated again referring to Fig. 3,

$$\Delta E/E = \cot \theta \Delta \theta$$

and

$$\Delta \theta = 4\alpha = \frac{w\theta}{2} \left[\frac{q-p}{pq} \right]$$

where i and the Bragg angle, θ are interchangeable.

These values of $\Delta\theta$ can then be used to calculate $A_{KB} = S.4\alpha$ for various choices of parameters. We consider the case of $p = 20 \text{ m}$, $q = 0.2 \text{ m}$ i.e. $M = 0.01$ and a single stage of magnification. We examine two Bragg reflectors: a Si(111) crystal and a multilayer coating with interplanar spacing of 20 \AA . First of all the geometrical acceptances A_{KB} are computed as before using the proper Bragg angle. Now in order to make a fair comparison two additional effects must be considered (1) The scattering efficiency of the multilayer is about 50% while for the Si(111) crystal, it is about 100%; (2) The intrinsic energy resolution of the multilayer is $1/n$ (in our case $1/50$) while the corresponding value for the Si(111) crystal is 1.3×10^{-4} . This gives the Si(111) crystal a disadvantage relative to the multilayer of a factor $1.3 \times 10^{-4} \times 50 = 6.5 \times 10^{-3}$ compared to the figure calculated above. If we adjust the geometrical acceptances downwards to allow for these "losses" we arrive at an "adjusted acceptance" which is plotted in Fig. 4. This allows our first conclusion which is that the multilayer is greatly superior to the silicon crystal for our present purpose. In understanding Fig. 4 we note that we are plotting limits. If we choose a particular reflector with fixed angle of incidence then of course the acceptance is a constant.

We have not yet considered the energy spreads resulting from a spot size based multilayer design or the spot sizes resulting from an energy spread based Si(111) design. In Fig. 5a we show the curvature driven energy spread for a multilayer whose width was chosen to achieve a 3μ spot. In Fig. 5b we show the spot size for a Si(111) crystal whose width was chosen to achieve a 2% energy spread. We again see that the multilayer is well matched to our purpose (the spread is everywhere less than 2%) while the spot size produced by the crystal blows up in an intolerable way.

THE ELLIPSOID OF REVOLUTION

An ellipsoid of revolution gives a perfect image of the axial object point limited only by fabrication tolerances and diffraction. It is well known that for off axis points the image quality degrades rapidly due to coma and if the mirror is a complete, 360° surface of revolution then an off axis point is imaged⁹ as an axial circle of such a radius as to pass through the gaussian image of the object point. This is obviously hopeless for microscopy but presents no problems at all for microprobe work. In fact, we would not want to make a complete 360° surface of revolution in part because the annular aperture of such a mirror could not be matched by the geometry of a synchrotron radiation source. Suppose we made a mirror of azimuthal angle ϕ . Then each point of the object is imaged as an arc 2ϕ whose center is the gaussian image of the object. If ϕ is large ($> 10^\circ$ say) then this effect produces the characteristic "bow tie" image of a normally shaped synchrotron source. For small ϕ there is very little smearing of the source shape.

Now since we are aiming for a 16 keV microprobe we should consider the ellipse geometry required to work with a grazing angle, $\theta = 6$ mr. The basic limit to fabricating this type of surface is that the radius (ρ) of rotation must not be too small. Let us suppose that a 10 mm radius is a practical limit then from simple geometry we arrive at a lower limit to the focal distance given by

$$f_{\min} = \frac{\rho}{2\theta}$$

For the present case this is 0.8 m so we see that it is only possible to fabricate the mirror if we have at least an 8m:0.8m system for 10:1 demagnification. This will make for a long beamline but is still feasible. The 100:1 ellipse is apparently not feasible.

The acceptance of this type of mirror is determined by the length and this is also limited by manufacturing considerations. Suppose we use the mirror to make a 3 μ spot at 0.8 m. The spot then subtends an angle 3.75 μ r at the mirror leading to a surface tolerance of about 1/3 arc, second! This is at the limit of what is possible even for small mirrors.

However, we do have one advantage. From the data in Fig. 1 it is clear that the width of the beam at the mirror will be no more than a few mm so the surface figure needs to be held to a close tolerance only over a narrow strip down the center of the mirror. With this encouragement let us optimistically say that a mirror 0.2 m long can be made.

With these figures we can now go ahead and calculate the details of the ellipsoid. The geometry for this is set out, for example, in Ref. 10. The numbers are given in Table 1. We see that the convergence angle at the focus is about 1.5 mr giving an acceptance of 4.5 mr. μ . We conclude that if an ellipsoid is used to form a 3 μ spot as the second stage of a two stage system then:

1. The ellipsoid is somewhat better than the KB system for forming the 3 μ spot but only by about a factor of 2.
2. The ellipsoid is what sets the limit to how much light can be accepted by the system and since this limit arises from manufacturing considerations, it is not possible to open up the aperture and trade flux for spot size: an important limitation.
3. From the "y co-ord" column in Table 1 we see that the minor radius changes by more than 10% indicating that a toroidal mirror (constant minor radius) would not be suitable.
4. The limited acceptance of the ellipsoid can be mitigated by choosing a lower energy limit than 16 keV. For example, for 5 keV ($\theta = 15$ mr) the value would be 28.6 mr. μ .

In the light 1 and 2 we may tentatively conclude that the extra cost and effort involved in introducing the ellipse as a second stage is not justified and the 100:1 KB appears to be the most cost effective system. Nevertheless, the two ellipse designs are shown on Fig. 4. We should note that a system with 3 μ spot, 4.5 mr. μ acceptance and overall magnification of 0.01 will collect only 0.015 mr from the source! It is obviously wasteful to use a source emitting into many mr for this purpose and it would be much more natural to look for wiggler/undulator configurations as sources for this type of experiment.

PRACTICAL BEAMLINE DESIGNS

Two general classes of beamline are available within the present technology; scanning (meaning that the point where the x-ray spot is delivered moves as the energy is varied) and constant deviation (fixed spot). At first glance the scanning system is not desirable because the detection systems, scanning stages and associated experimental hardware are inevitably bulky and a scanning system would require complex engineering to achieve the necessary precise motions. On the other hand the constant deviation design has considerable problems. It requires two stages of demagnification if an ellipse is used as the second stage to achieve the largest possible acceptance and in that case an extra optical element is needed. Furthermore, if one of the elements is to be a multilayer at fixed deviation, a graded interplanar spacing must be used to vary the reflected energy at fixed Bragg angle. Such graded spacings have been produced⁸ but they are still far from routine. The counterpart of this in the scanning system is a multilayer with fixed spacing. This is simpler to make but it is now necessary to tune the radius of curvature of the reflector surface to the right value to be in focus at any particular Bragg angle. This can be done but is certainly an added complication. The scanning device has some additional advantages for the lower energies required to span all the elements to $Z = 86$ or so. At fixed angle, a tungsten-carbon multilayer set to Bragg reflect 16 keV photons with $d = 20 \text{ \AA}$, will totally externally reflect photons at an energy of $\sim 5 \text{ keV}$ and below. Thus for photon energies below 5 keV the fixed deviation multilayer no longer acts as a monochromator. Another totally different strategy would be to carry out monochromatization and focusing in a completely separate device with the concomitant loss in intensity. Clearly, scanning and constant deviation systems have both advantages and technical challenges and we should keep both as options in our thinking.

The most favorable arrangement in both systems uses a 100:1 single stage demagnification with a multilayer coated Kirkpatrick-Baez mirror to focus and monochromate in the horizontal plane and a 100:1 specular reflector to focus in the vertical. The performance of this system is only slightly worse than the ellipse as can be seen from Fig. 5. The instrument is shown schematically in Fig. 8. It can be made constant deviation by using a variable d -spacing multilayer or scanning by using a constant d -spacing multilayer with tunable radius. At the present time it seems that the simplest scheme that meets all our scientific requirements is a

horizontally focusing scanning multilayer, $d = 20 \text{ \AA}$, $f = 0.2 \text{ m}$ followed by a vertically focusing mirror again giving a 3 \mu m spot with $f = 0.1 \text{ m}$. In order to scan the full energy range the incidence angle on the multilayer would vary from 1.10° to 8.91° . This implies that the focal spot would move through a horizontal arc of radius 0.2 m and angle 15.62° . The experiment and the vertically focusing mirror are therefore mounted on an arm driven by a $\theta/2\theta$ drive which also drives the Bragg angle at the multilayer.

ACKNOWLEDGEMENT

One of us (MRH) wishes to acknowledge advice and help from J. Kirz who originally stimulated his interest in this problem.

References

1. C.J. Sparks, Jr., Chapter 14, Synchrotron Radiation Research, H. Winnick, S. Doniach (Eds.), Plenum, New York, 1980.
2. B.M. Gordon, Proc. 4th Intl. Conf. Nuclear Methods in Environmental and Energy Research, Columbia, MO, April 1980.
3. B.M. Gordon, private communication.
4. P. Kirkpatrick and A.V. Baez, JOSA 38, 9, 766 (1948).
5. J. Dymon, Proc. Phys. Soc. Lond. B, 65, 580 (1952).
6. J.F. McGee and J.W. Milton, X-ray microscopy and microlithography, Engstrom, Cosslett and Pattee (Eds.), Elsevier, Amsterdam (1960).
7. R.H. Price in Conf. on Low Energy X-ray Diagnostics, Monterey, 1981, American Institute of Physics, Conference Proceedings #75, D. Attwood and B. Henke (Eds.)
8. D.J. Nagle, T.W. Barbee, J.V. Gilfrich, Proc. SPIE, Vol. 315.
9. H. Wolter, Ann. Phys. 10, 94 (1952).
10. M.R. Howells, Brookhaven report #27416.
11. T.W. Barbee, Loc. cit. ref. 7.

Figure Captions

Fig. 1. Limiting emittances/acceptances:

- A. x-ray ring
- B. VUV ring
- C. Reflectance limit
 $A_R = 0.5 \theta_c \cdot x$ where $x = 3 \mu\text{m}$
- D. Global diffraction limit
- E. Acceptance limit of a gold zone plate whose nominally opaque regions actually transmit 10%.
- F. Maximum emittance for which the spot size limited resolution is not spoiled by the beam divergence (sample = protein, spot = 3μ)

Fig. 2. Kirkpatrick Baez x-ray microscope.

Fig. 3. Notation for discussing the geometry of the Kirkpatrick Baez microscope.

Fig. 4. Comparison of the acceptances of various optical elements for a microprobe. See text for meaning of acceptance in this case.

- A. x-ray ring emittance
- B. Kirkpatrick Baez (specular reflector); $30 \mu\text{m}$ spot, $f = 1 \text{ m}$
- C. 5 keV ellipse (specular reflector); $3 \mu\text{m}$ spot
- D. Multilayer; $3 \mu\text{m}$ spot, $f = 0.2 \text{ m}$, $d = 20 \text{ \AA}$
- E. 15 keV ellipse (specular reflector); $3 \mu\text{m}$ spot
- F. Kirkpatrick Baez (specular reflector); $3 \mu\text{m}$ spot, $f = 0.1 \text{ m}$
- G. Si(111) crystal; $3 \mu\text{m}$ spot, $f = 0.2 \text{ m}$

Fig. 5. A. Spatial aberration (S) for Si(111) KB with $\Delta E/E = 0.01$; $f = 0.2 \text{ m}$

- B. Geometric contribution to energy spread ($\Delta E/E$) for 20 \AA d-spacing multilayer designed for $f = 0.1 \text{ m}$ and $3 \mu\text{m}$ spot size.

Fig. 6. Suggested beamline layout for microprobe using Kirkpatrick-Baez optics.

- M1: Multilayer: $f = 0.2 \text{ m}$; 3μ aberration limit fixed deviation with a graded spacing or variable deviation with fixed spacing and variable radius
- M2: Specular mirror: $f = 0.1 \text{ m}$; $3 \mu\text{m}$ aberration limit

Table I. Ellipse Parameters

$r = 8000$ mm
 $r' = 800$ mm
 $\theta = 89.656$ deg.
 Grazing angle: 6.0 mr

Mirror Full Length = 200 mm

Major Axis = 4400 mm
 Minor Axis = 15.178 mm
 Eccentricity = 0.999994049641
 Mirror Center XO = 3600.021 mm
 Mirror Center YO = 8.727 mm
 Magnification = 0.1
 Center Curvature = 242425.7 mm
 Convergence Angle at Focus = 1.51 mr

<u>Dist. From Center</u>	<u>Y Co-ord</u>	<u>Diff. From St. Line</u>	<u>Diff. From Circle</u>	<u>Angle To Axis</u>	<u>Angle Of Incidence</u>
-100.00	9.1985	.0195	-.00108	.58560	.32616
- 80.00	9.1072	.0126	-.00056	.59297	.32943
- 60.00	9.0145	.0072	-.00024	.60058	.33282
- 40.00	8.9203	.0032	-.00007	.60846	.33633
- 20.00	8.8245	.0008	-.00001	.61660	.33998
0.00	8.7271	.0000	.00000	.62505	.34377
20.00	8.6281	.0008	.00001	.63380	.34772
40.00	8.5274	.0034	.00008	.64288	.35183
60.00	8.4249	.0077	.00026	.65232	.35611
80.00	8.3205	.0138	.00063	.66214	.36057
100.00	8.2143	.0219	.00126	.67237	.36524

Distances in mm, angles in degrees

Table II. Ellipse Parameters

$r = 3333.333$ mm
 $r' = 333.333$ mm
 $\theta = 89.140$ deg.
 Grazing angle: 15.0 mr

Mirror Full Length = 200 mm

Major Axis = 1833.333 mm
 Minor Axis = 15.810 mm
 Eccentricity = 0.99996281202
 Mirror Center XO = 1500.055 mm
 Mirror Center YO = 9.089 mm
 Magnification = 0.1
 Center Curvature = 40405.5 mm
 Convergence Angle at Focus = 9.52 mr

<u>Dist.</u> <u>From</u> <u>Center</u>	<u>Y</u> <u>Co-ord</u>	<u>Diff.</u> <u>From</u> <u>St. Line</u>	<u>Diff.</u> <u>From</u> <u>Circle</u>	<u>Angle</u> <u>To</u> <u>Axis</u>	<u>Angle</u> <u>Of</u> <u>Incidence</u>
-100.00	10.2076	.1096	-.01411	1.34980	.76534
- 80.00	10.0000	.0717	-.00745	1.38634	.78123
- 60.00	9.7850	.0413	-.00324	1.42551	.79839
- 40.00	9.5620	.0188	-.00099	1.46766	.81701
- 20.00	9.3305	.0048	-.00013	1.51320	.83727
0.00	9.0899	-.0000	-.00000	1.56263	.85944
20.00	8.8393	.0051	.00014	1.61656	.88379
40.00	8.5780	.0210	.00116	1.67574	.91072
60.00	8.3048	.0486	.00408	1.75110	.94066
80.00	8.0187	.0893	.01010	1.81385	.97423
100.00	7.7181	.1444	.02068	1.89552	1.01216

Distances in mm, angles in degrees

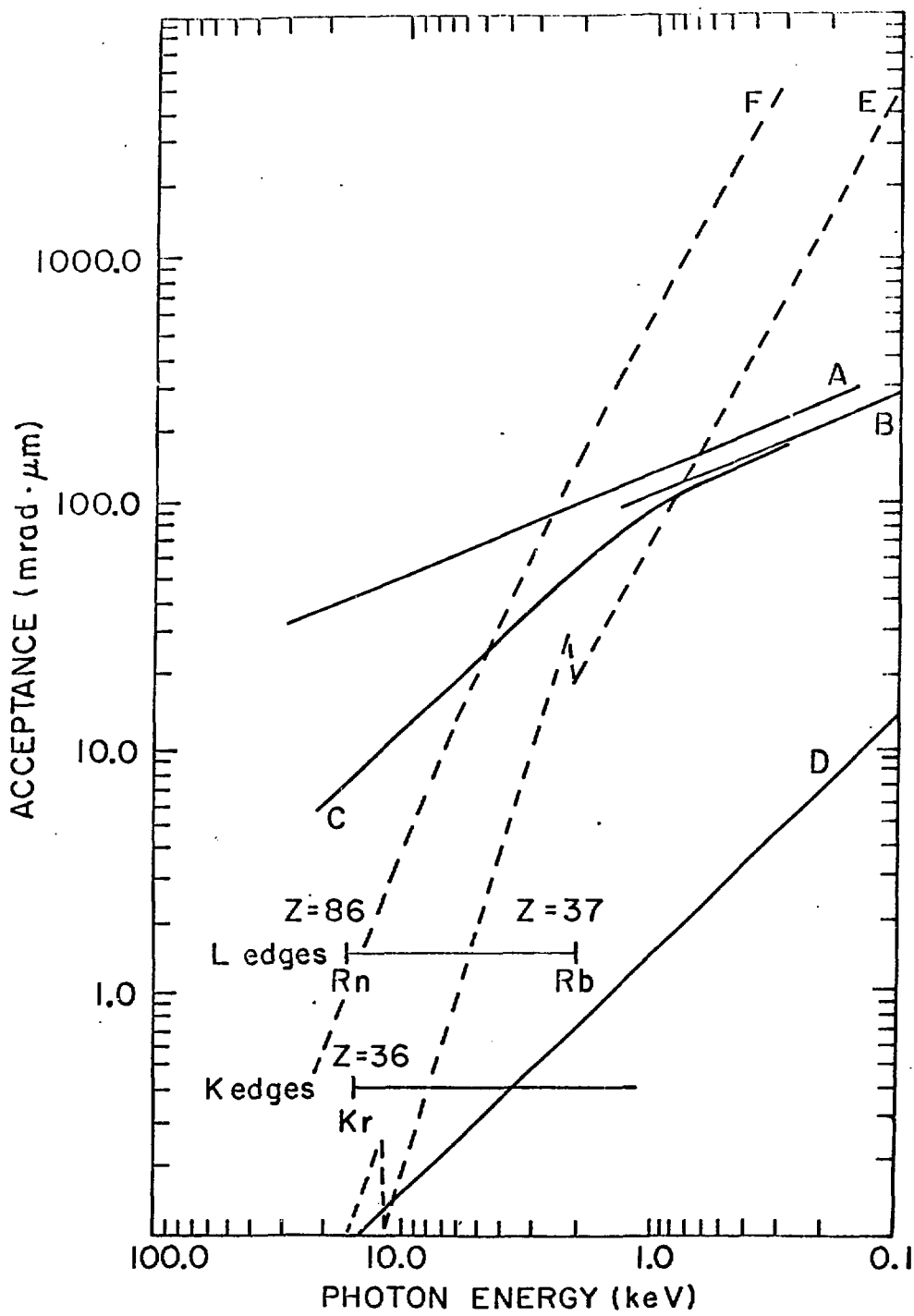


Fig. 1

KIRKPATRICK BAEZ MICROSCOPE :

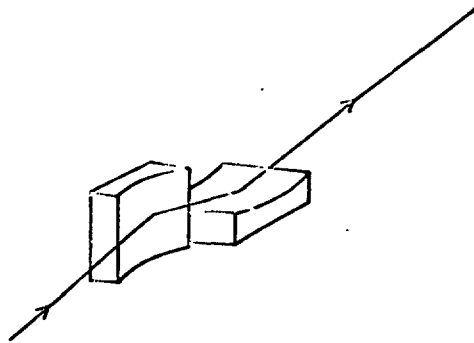


Fig. 2

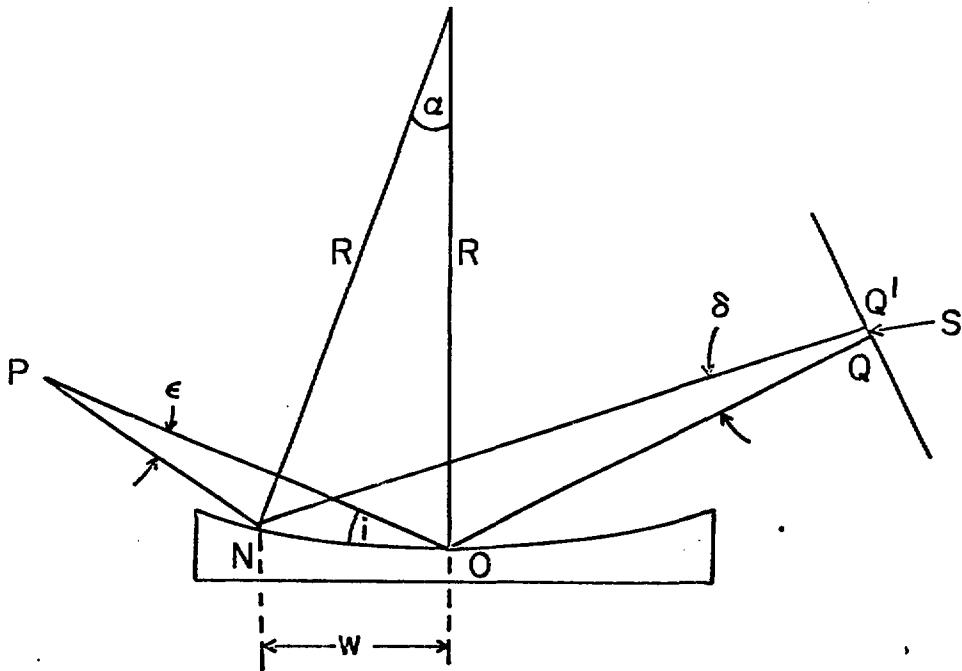


Fig. 3

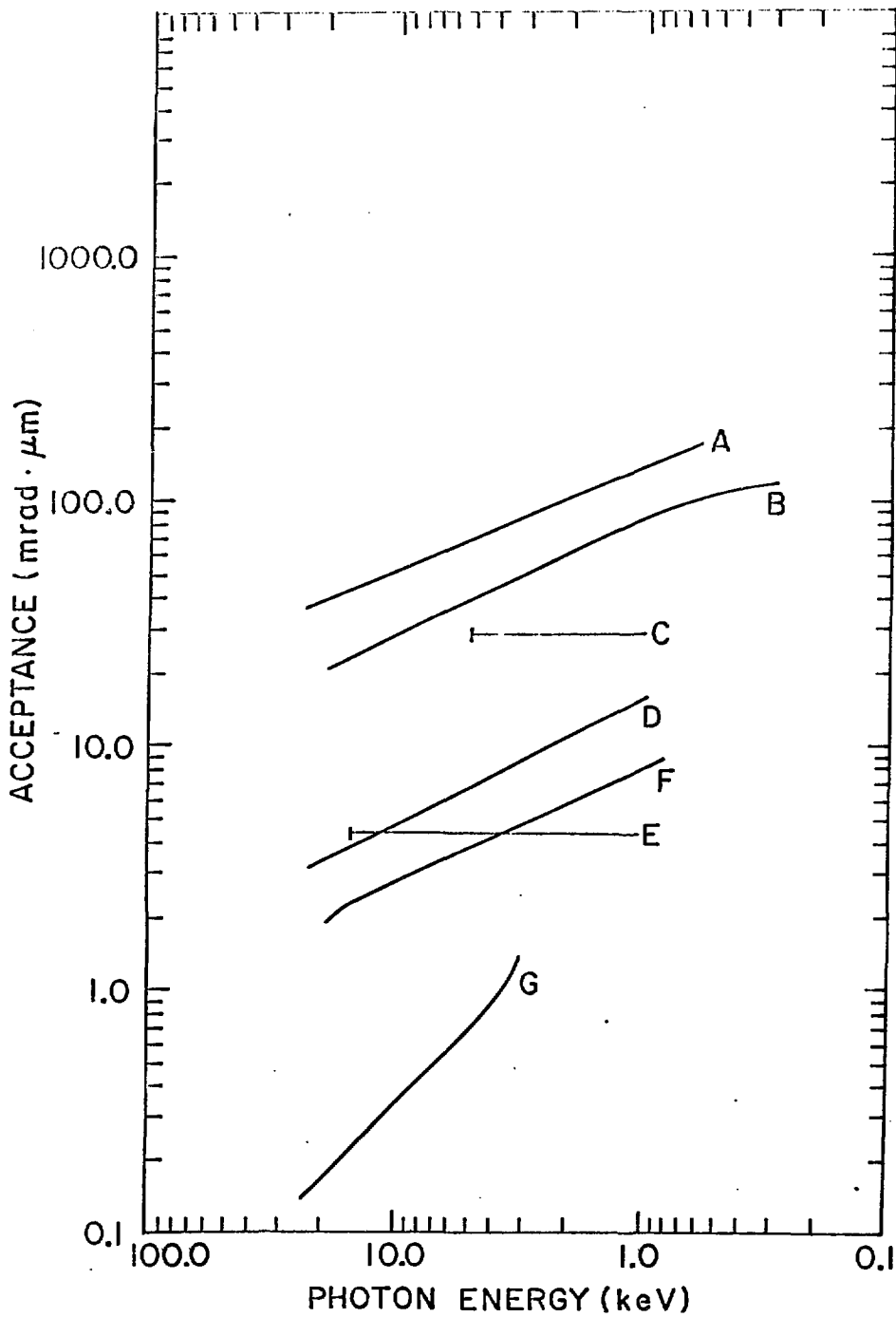


Fig. 4

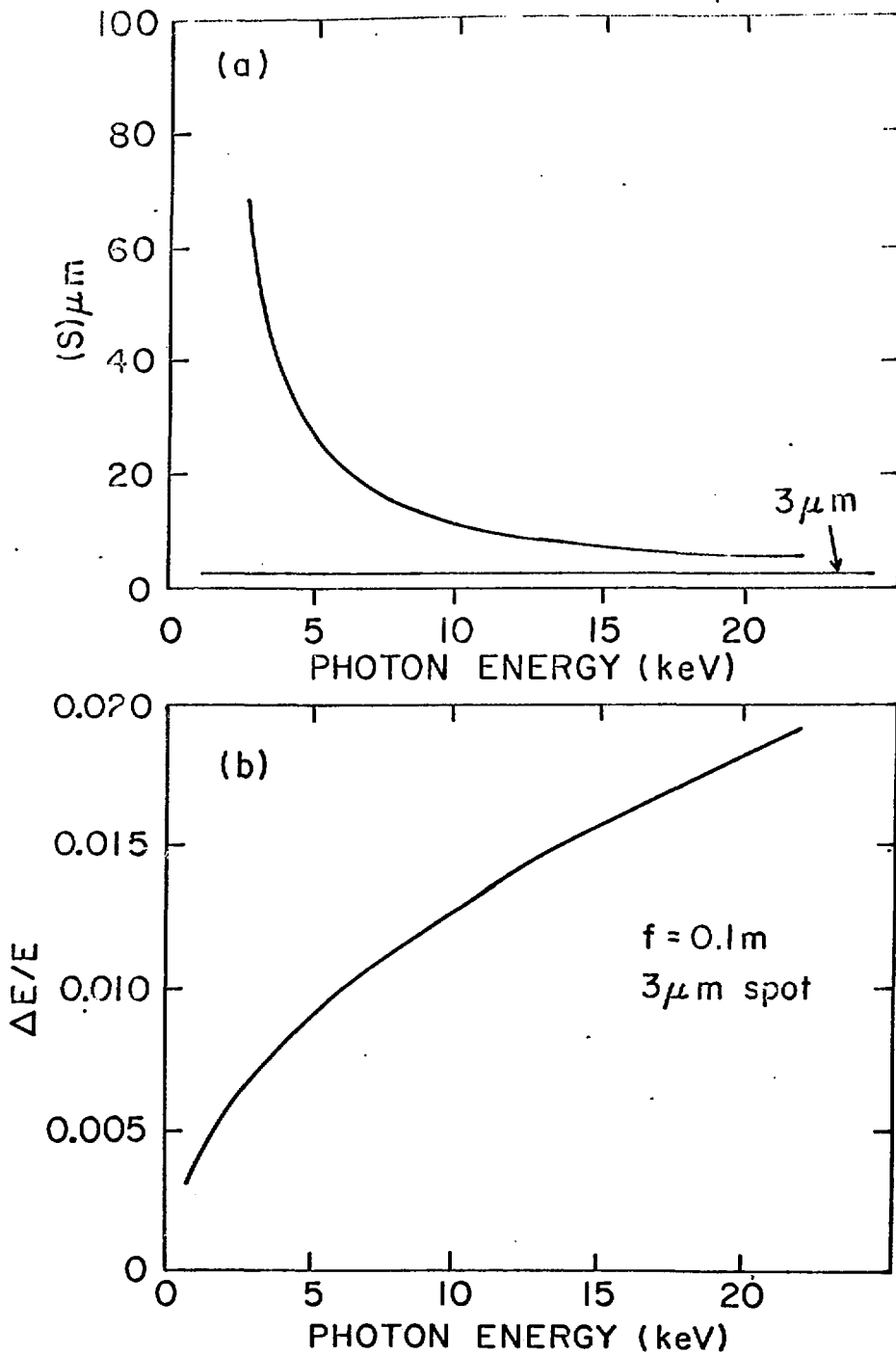
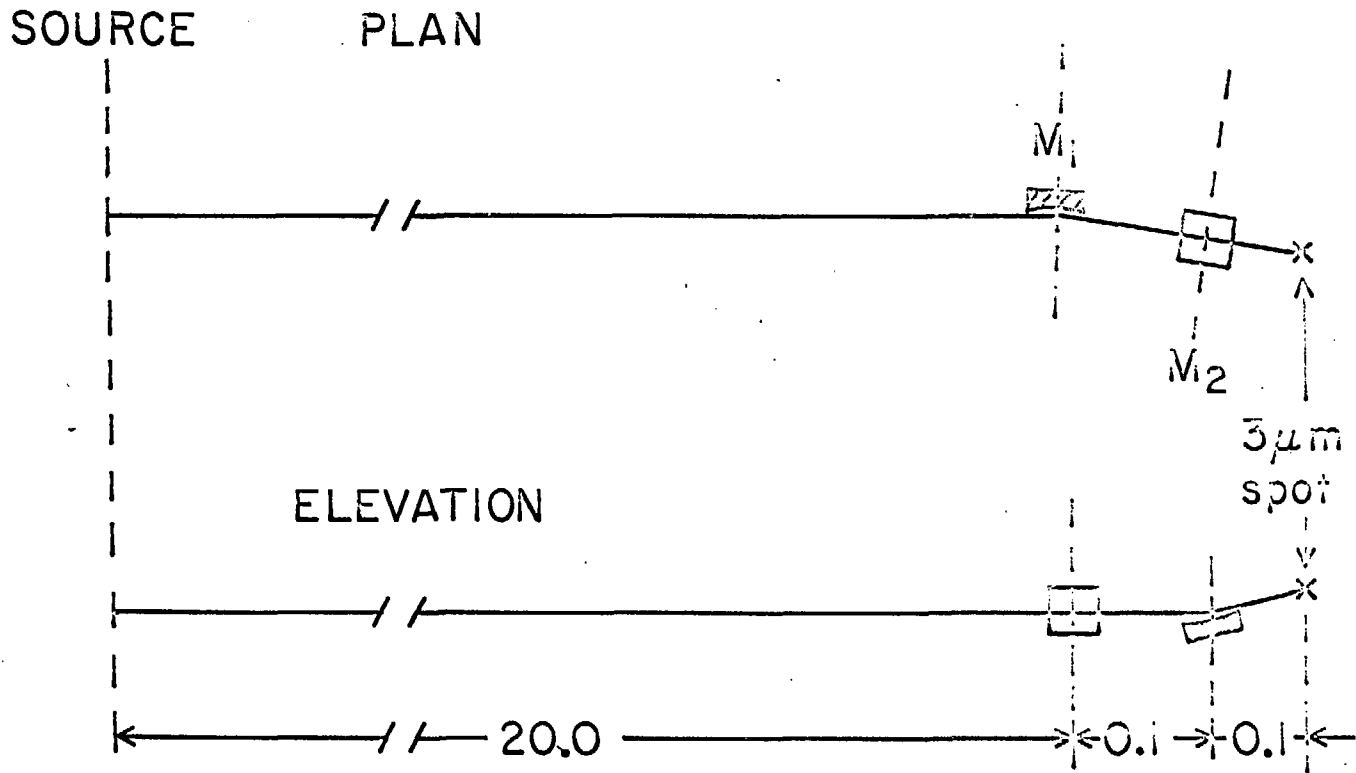


Fig. 5



NOT TO SCALE
DISTANCES IN m

Fig. 6